Applied Surface Science 614 (2023) 156171

Contents lists available at ScienceDirect

Applied Surface Science

journal homepage: www.elsevier.com/locate/apsusc

Full Length Article

# Evolution of surface and bulk structure of supported palladium nanoparticles by *in situ* X-ray absorption and infrared spectroscopies: Effect of temperature, CO and $CH_4$ gas

Oleg A. Usoltsev [a,*], Alina A. Skorynina [a], Bogdan O. Protsenko [a], Vlad Martin-Diaconescu [b], Riccardo Pellegrini [c], Alexander V. Soldatov [a], Jeroen van Bokhoven [d,e], Aram L. Bugaev [a]

[a] The Smart Materials Research Institute, Southern Federal University, Sladkova, 178/24, 344090 Rostov-on-Don, Russia
[b] CELLS-ALBA Synchrotron Radiation Facility, Carrer de la, Llum 2-26, 08290 Cerdanyola del Vallès, Spain
[c] Chimet S.p.A. - Catalyst Division, Via di Pescaiola, 74, 52041 Viciomaggio Arezzo, Italy
[d] Laboratory for Catalysis and Sustainable Chemistry, Paul Scherrer Institute, 5232 Villigen, Switzerland
[e] Institute for Chemical and Bioengineering, ETH Zurich, Vladimir-Prelog, Weg 1, 8093 Zurich, Switzerland

ARTICLE INFO

*Keywords:*
Palladium nanoparticles
Palladium carbides
CO
XANES
DRIFTS

ABSTRACT

Interaction of CO and $CH_4$ with palladium is a relevant process in numerous catalytic reactions, which may induce structural changes in the metal affecting its catalytic properties This work establishes a systematic study of the evolution of the atomic and electronic structure in alumina- and carbon-supported palladium nanoparticles in presence of CO and $CH_4$ gases at temperatures from 50 to 350 °C by a combination of *in situ* X-ray absorption and infrared spectroscopies. Immediate adsorption of CO molecules with formation of surface carbon deposits due to the disproportionation reaction occurs at low temperatures, while above 250 °C, active formation of bulk palladium carbide is observed. In $CH_4$ the later process starts only at ca. 350 °C. Reduction of palladium and contraction of the Pd-Pd interatomic distances were observed with increasing temperature irrespective of the gas atmosphere, including the inert one, particle size and the type of support. For carbon supported samples formation of palladium carbide occurred above 200 °C due to the decomposition of the support.

## 1. Introduction

Interaction of CO and $CH_4$ with palladium is a problem of high practical relevance, since, on the one hand, palladium-containing catalysts are extensively used in $CH_4$ selective oxidation [1,2] and combustion [3–7], and CO combustion [8–11]. On the other hand, CO and $CH_4$ can be present as intermediates in numerous reactions, such as $CO_2$ hydrogenation [12–14] and others. It can be expected that the catalyst's surface, as well as its bulk structure, can undergo structural changes as a function of the composition of gaseous atmosphere, temperature, and time which makes *in situ* and *operando* experiments of utmost importance [11,14,15]. For example, interaction of palladium with hydrogen is known for decades [16], and based on the known Pd-H phase diagram, a researcher can optimize reaction conditions and correlate the catalyst behavior with metallic or hydride phase of palladium. Unlike palladium hydride phase, the "phase diagrams" of palladium carbides are not established and the result of interaction of palladium nanoparticles with a potential source of carbon, such as CO or $CH_4$ molecules, is apriori unknown.

In a number of works, evolution of the structure of palladium-based catalysts exposed to CO, $CH_4$ and various reaction mixtures was followed by X-ray based techniques, namely X-ray absorption spectroscopy (XAS) and X-ray diffraction (XRD) [2,4,5,11,15]. However, such techniques are least sensitive to light impurities, like carbon, in the palladium lattice, and the detection of Pd-C interaction requires specific analytical approaches to be adopted [17–23]. The main advantage of X-ray techniques is their versatile application under *in situ* and *operando* conditions, including high pressures, due to utilization of high energy photons. Both XAS and XRD are bulk-sensitive, but since XAS does not require long-range order, its application to small (1–3 nm) nanoparticles allows extracting information about both surface and bulk of the particles [17,18], while XRD often fails in the detection of ultra-small (below 2 nm) nanoparticles [24], as well as in the cases of crystalline supports that can overshadow the reflections related to the supported particles

* Corresponding author.
*E-mail address:* oleg-usol@yandex.ru (O.A. Usoltsev).

https://doi.org/10.1016/j.apsusc.2022.156171
Received 15 August 2022; Received in revised form 13 December 2022; Accepted 19 December 2022
Available online 20 December 2022

[23,25]. In the case of palladium, Pd *K*-edge XAS (~24 keV) is widely applied, which probes the transition from 1 *s* to the unoccupied *p*-states. In this case, extended X-ray absorption fine structure spectroscopy (EXAFS) spectra provide the (averaged) information about the local geometry around palladium atoms: coordination numbers, interatomic distances, and Debye-Waller parameters. Although *p*-states are less sensitive to the chemical surrounding compared to *d*-states, not only the oxidation state of Pd, but also the type of ligands and light impurities (H, C, N, O) can be determined by the analysis of X-ray absorption near-edge structure (XANES) [19–22]. Diffuse reflectance infrared Fourier transform spectroscopy (DRIFTS) [2,6,7,10] is often used as an independent and complementary to XAS tool for *in situ* and *operando* characterization via the vibrational properties of the probe molecules, such as CO, adsorbed on the active sites of the catalyst. A DRIFTS spectrum is therefore sensitive to the type and chemical state of the adsorption site, as well as the adsorption geometry.

In this work, we investigate in detail the evolution of relevant industrial catalysts, represented by alumina- and carbon-supported palladium nanoparticles, upon interaction with CO and $CH_4$ gases in the temperature range from 50 to 350 °C. We reveal the role of CO (Section 3.1), $CH_4$ (Section 3.2), the temperature effect and the type of support (Section 3.3) on the local atomic and electronic structure of palladium by combination of *in situ* XANES, EXAFS and DRIFTS spectroscopies. The used multi-technique approach allowed us to follow the evolution of both surface and bulk of the particles.

## 2. Methods

**Commercial $Pd/Al_2O_3$, Pd/C and Pd/P4VP samples** were provided by Chimet S.p.A. and have been extensively characterized in a series of previous works [19,26–28]. Alumina- and carbon-supported samples were prepared by a deposition–precipitation using $Na_2PdCl_4$ as the metal precursor (5 wt% Pd with respect to the support) and $Na_2CO_3$ as the basic agent. The catalysts were pre-reduced by sodium formate at 65 °C for 1 h, carefully washed with water for complete removal of chlorine residues and dried overnight at 110 °C. Both samples have the resulting metal loading of 5 wt% with the average particle size of ca. 3 nm. In addition, sample of Pd nanoparticles with ca. 1 nm particle size on poly-4-vinylpyridine (P4VP) support was used (see Section S1 of the Supporting Information).

***In situ* Pd *K*-edge XAS measurements** were performed at CLAESS beamline of ALBA synchrotron (Barcelona, Spain) [29]. Around 80 mg of $Pd/A_2O_3$ and 40 mg of Pd/C samples were pelletized and loaded into *in situ* cell (ITQ-ALBA Multipurpose Cell, Fig. S1) allowing for the remote control of gas flow and temperature during XAS measurements (for Pd/C sample the powder was pressed directly into the sample holder). The heating was performed by cartridge heaters implemented in the cell and monitored by a thermocouple located inside the reaction zone. Prior to every experimental procedure, the fresh sample was taken and activated in 50 mL/min flow of 20 % $H_2$/He at 125 °C for 30 min and then purged by He flow to ensure the initial metallic state of palladium particles. The procedure for Pd/P4VP sample is described in Section S1 of the Supporting Information.

XAS spectra were collected in transmission geometry using Si (3 1 1) double-crystal monochromator operated in the continuous scanning mode with averaged measurement time of ca. 1.5 min per spectrum. Higher harmonics were cut by collimating mirrors located after the monochromator. Beam intensity before ($I_0$) and after ($I_1$) the sample was measured by ionization chambers. The third ionization chamber was used to simultaneously measure the intensity $I_3$ after the reference palladium foil for energy calibration.

**XAS data processing** including energy calibration, normalization, background removal and first-shell Fourier-analysis were performed in a self-written python script utilizing the larch library [30]. The fist-shell fitting of the Fourier-transformed (FT) data was performed independently for each spectrum using the interatomic distance ($R_{Pd\text{-}Pd}$), Debye-Waller factor ($\sigma_{Pd\text{-}Pd}$), coordination number ($N_{Pd\text{-}Pd}$) and zero energy shift ($\Delta E_0$) as fitting variables. The photoelectron backscattering phases and amplitudes were calculated by FEFF6 code [31,32]. Principle component analysis (PCA) and multivariate curve resolution (MCR) were applied to XANES spectra using PyFitIt code [33]. *Ab initio* calculation of XANES spectra was performed in the FDMNES code [34,35] (See Section S3 in the Supporting Information).

***In situ* DRIFTS measurements** for $Pd/Al_2O_3$ sample were performed on Bruker Vertex 70 spectrometer equipped with a highly sensitive liquid mercury telluride detector. All spectra were recorded in the 5000–400 $cm^{-1}$ range with a resolution of 1 $cm^{-1}$ and accumulated for 1 min. The adsorption spectra were obtained using the Kubelka-Munk function. Around 12 mg of sample in the form of powder was loaded into the Praying Mantis low temperature reaction chamber (Harrick Scientific Products Inc., New York, USA) for DRIFTS measurements under controlled temperature and gas flow. The cell was heated by an electric furnace. Temperature was measured by the thermocouple placed on the outer wall of the microreactor and controlled by the Thermodat-17 thermocontroller. An external gas delivery system equipped with mass flow controllers (EL-FLOW, Bronkhorst High-Tech B.V., Ruurlo, Netherlands) operated by a python script was used to set the flows of He, $H_2$, and CO through the cell. Like in the XAS experiment, the sample was first activated for 30 min at 125 °C in the 50 mL/min flow of 20 % $H_2$/He and then cooled down to 50 °C in He (50 mL/min). The spectrum collected under these conditions was used as a background for all the following spectra. The flow was then switched to 5 % CO in He with total flow of 50 mL/min and the cell was heated to 330 °C with ramp of 5 °C/min. The spectra were collected continuously with the time-step of ca. 1 min. The spectra processing was also performed by a self-written python script allowing for reading the Bruker Opus file format, subtraction of the background (activated sample before CO), automatic detection of the adsorbed CO peaks' positions and PCA and MCR analysis. The details of DRIFTS data processing are given in Section S2 of the supporting information.

## 3. Results

### 3.1. $Pd/Al_2O_3$ catalyst upon heating in CO

Two types of changes were observed in the XANES spectra upon heating the $Pd/Al_2O_3$ sample in the constant flow of 10 %CO/He (Fig. 1a, Figs. S3–S4): (i) a gradual shift of all maxima and minima towards higher energies up to 250 °C and back to lower energies for higher temperatures, and (ii) a broadening of the first maximum at ca. 24.36 keV towards higher energies. The former effect can be explained by the changes in the Pd-Pd interatomic distances which was also observed in EXAFS data (vide infra). The latter, indicative for the changes in the electronic structure of the unoccupied *p*-states of palladium, was further evidenced in the difference XANES spectra (Fig. 1a and Fig. S4), where the peak at ca. 24.37 keV was observed. Similar changes were previously reported to be indicative for the Pd-C bond formation during adsorption of hydrocarbons and formation of palladium carbides [21,26–28]. The PCA analysis of XANES (Fig. S13a) revealed the existence of three independent phases (based on the scree plot and visual comparison of the obtained components), and the MCR analysis provided the evolution of three independent species (Fig. 1b) with the corresponding XANES spectra (Fig. 1c). To appreciate the small changes in the shape of XANES, the difference spectra were constructed in the same figure (magnified by 10 with respect to the pristine spectra) by subtracting a spectrum of the pure metallic state of $Pd/Al_2O_3$ after activation. A gradual decrease of the first component (blue data in Fig. 1b,c) was observed upon heating with simultaneous growth of the second one. Both components share similar spectral features, however, in the blue one, the changes in the near-edge region that resulted in a minimum and a maximum at 24.35 and 24.37 keV, respectively, in the difference spectra are stronger, while in the black one, a bigger difference with respect to the metallic state is

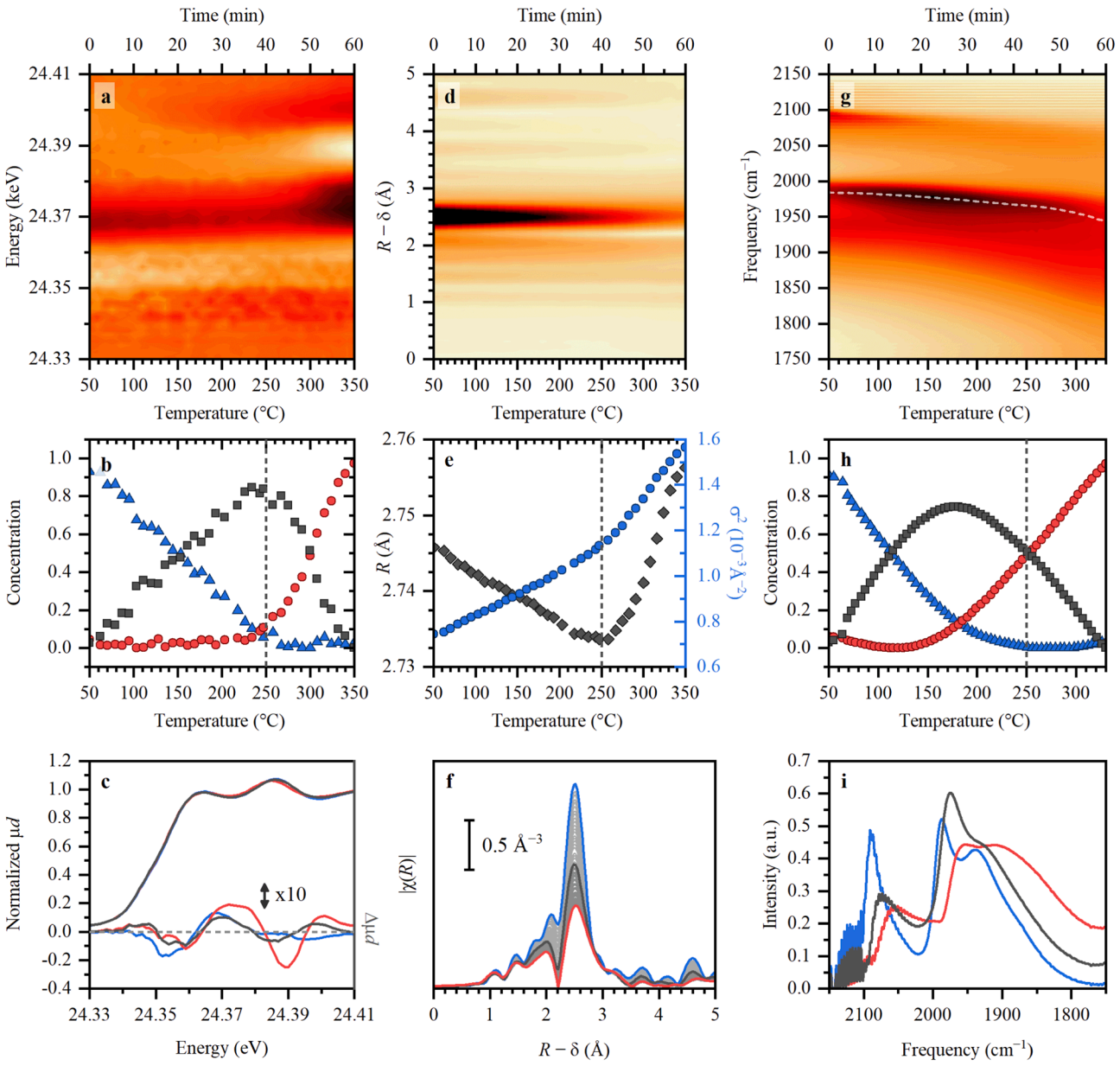


**Fig. 1.** Evolution of the experimental data for $Pd/Al_2O_3$ upon heating in CO. (a) Difference XANES spectra, obtained by subtracting the spectrum of pure metallic state of $Pd/Al_2O_3$, concentration profiles (b) and spectra with corresponding difference spectra (c) obtained from MCR analysis. (d) FT-EXAFS data (phase uncorrected). (e) Refined values of the first-shell Pd-Pd interatomic distances (black diamonds, left axis) and Debye-Waller parameter (blue circles, right axis). (f) FT-EXAFS spectra (phase uncorrected), with blue, black and red lines corresponding to 50, 250 and 350 °C, respectively. (g) DRIFTS spectra after background subtraction, concentration profiles (h) and spectra (i) obtained from MCR analysis. (For interpretation of the references to colour in this figure legend, the reader is referred to the web version of this article.)

observed in the region around 24.38 keV. The appearance and growth of the third component were observed above 250 °C. This component is characterized by a shift of the first peak towards higher energies, resulting in a maximum in the difference spectrum at 24.37 eV, and the shift of the following peaks towards lower energies, which is associated with the increase of the Pd-Pd interatomic distances.

In FT-EXAFS data, a decreasing peak at ca. 2.5 Å (phase-uncorrected) was observed (Fig. 1, parts d and f) corresponding to the first-shell Pd-Pd contribution. The fitting performed on the whole dataset explained this behavior by the increasing Debye-Waller parameter. This increase was linear with temperature in 50–250 °C range, and a stronger growth was observed above 250 °C. The Pd-Pd interatomic distances were first decreasing, reaching a minimal value of ca. 2.73 Å at 250 °C and then increased up to ca. 2.76 Å at 350 °C.

DRIFTS spectra collected under identical conditions were characterized by several bands in 1750–1850 $cm^{-1}$ range (Fig. 1g and Fig. S9) corresponding to the vibrations of the adsorbed CO molecules in addition to the signal of the gas phase CO. All peaks were red-shifted upon heating, with the strongest effect observed for the peak originally located at 1985 $cm^{-1}$ assigned to a bridged CO [36]. The position of the latter, highlighted by dashed grey line in Fig. 1g, shifts linearly with temperature in the 50–250 °C range, and then demonstrates a stronger decrease, which correlates qualitatively with the changes observed in XANES and EXAFS spectra. As in XANES, MCR analysis was applied to obtain the DRIFTS spectra of pure species and their concentration profiles (Fig. 1h,i). The behavior of the three components is similar to that determined for XANES spectra (Fig. 1b), however, the maximum of the intermediate one (black squares) is observed at lower temperature

(around 180 °C). This component is also characterized by the relative increase of the intensity of the bridge CO vibration in 1950–2000 $cm^{-1}$ region. After heating to 350 °C, the intensities of linear (2000–2100 $cm^{-1}$) and bridge CO are decreased, while the hollow one (at ca. 1900 $cm^{-1}$) is preserved comparing to the initial state at 50 °C.

### 3.2. $Pd/Al_2O_3$ catalyst upon heating in $CH_4$

As in the case of CO, two types of changes were observed in XANES spectra in presence of $CH_4$ gas, but the exact temperature ranges for the corresponding changes were different. Monotonous contraction of Pd-Pd distances from 2.75 to 2.72 Å accompanied by a linear growth of the Debye-Waller parameter is observed upon heating up to 350 °C (Fig. 2a, left side). However, further action of $CH_4$ at 350 °C (Fig. 2a, right side) resulted in the increase of Pd-Pd distances back to 2.75 Å with the increase of the Debye-Waller. Again, three components were observed in XANES spectra by PCA analysis (Fig. S7b). The behavior of their concentration profiles is similar to the case of CO, but the growth of the final carbide-like component is observed only at 350 °C (Fig. 2b). The exact shape of the MCR-components is different from those obtained for CO case, which can be also seen by comparing the original experimental spectra measured after CO and $CH_4$ exposure at room temperature (Fig. S5a), while the resulting state at 350 °C is similar for the two gasses.

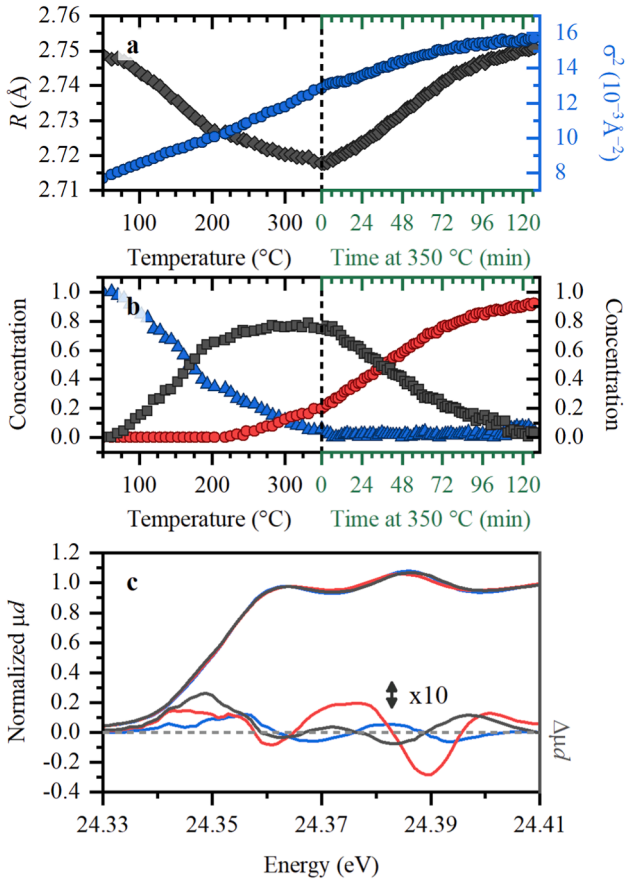


**Fig. 2.** Evolution of (a) the first-shell Pd-Pd interatomic distances (black diamonds, left axis) and Debye-Waller parameter (blue circles, right axis), and (b) concentration profiles of three MCR components whose XANES and difference XANES spectra are shown in panel (c) (left and right axes, respectively) upon heating in $CH_4$ flow. (For interpretation of the references to colour in this figure legend, the reader is referred to the web version of this article.)

### 3.3. $Pd/Al_2O_3$ and Pd/C catalysts upon heating in He

To focus on the contraction of interatomic distances, heating in inert atmosphere was performed for alumina (the same as in previous subsections) and carbon supported catalysts (particle size of ca. 3 nm in both samples). A linear decrease of Pd-Pd distances with a linear increase of the Debye-Waller parameter (Fig. 3a, solid black diamonds and solid blue circles, respectively) was observed for $Pd/Al_2O_3$ sample upon heating in the whole temperature range. Exactly the same trend was obtained for the Pd/C sample for the temperatures up to 200 °C (hollow black diamonds and blue crosses in Fig. 3a). In XANES data, apart from the shift of the second peak at 24.39 keV towards higher energies, associated with the decrease of interatomic distances, a slight shift of the edge position towards lower energies was observed (Fig. 3b and Fig. S6a, data for $Pd/Al_2O_3$). For carbon supported sample, heating above 200 °C induced a sudden increase of interatomic distances not registered for the alumina supported one. At the same time the shape of XANES spectrum after heating (Fig. S6b) was similar to that of palladium carbide, which can be caused by a decomposition of the carbon support.

## 4. Discussion

The presented results allow one to interpret the evolution of palladium structure upon external stimuli based on the data from three complementary techniques. EXAFS spectra are sensitive to the structure of the palladium framework: averaged interatomic distances, Debye-Waller parameters, and coordination numbers. XANES spectra are affected by both atomic and electronic local structure of palladium atoms, including formation of palladium carbides and adsorption of the reactive molecules on the nanoparticle's surface. DRIFTS data reflect the morphology of the surface and the electronic state of surface Pd sites by monitoring the changes in the vibrational properties of the adsorbed CO

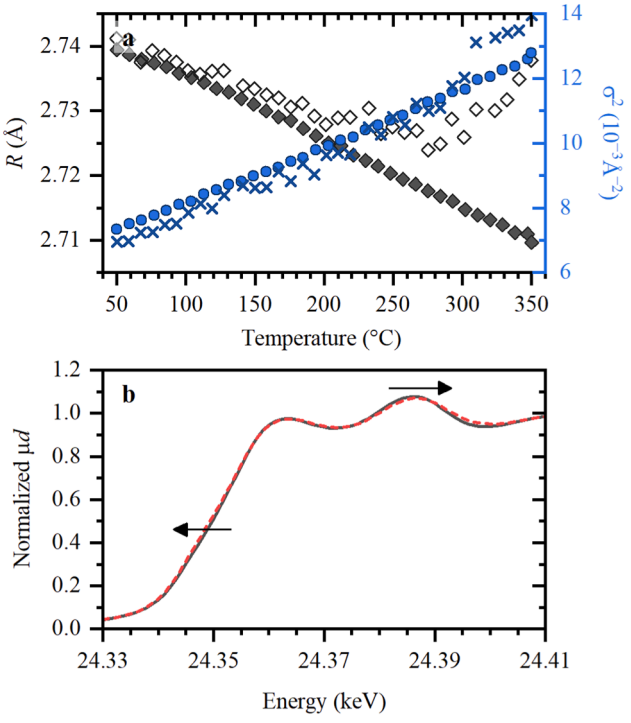


**Fig. 3.** (a): Evolution of the first shell Pd-Pd interatomic distances (left axis, solid and hollow black diamonds for $Pd/Al_2O_3$ and Pd/C, respectively) and Debye-Waller parameter (right axis, solid blue circles, and blue crosses for $Pd/Al_2O_3$ and Pd/C, respectively) and (b): Initial (solid black) and final (dashed red) XANES spectra for $Pd/Al_2O_3$ upon heating in He. (For interpretation of the references to colour in this figure legend, the reader is referred to the web version of this article.)

molecules. For the discussion below, it is important to consider that for the particle size of ca. 3 nm, EXAFS and XANES data are equally sensitive to both surface and bulk structure of the nanoparticles.

### 4.1. Evolution of CO on palladium nanoparticles

The data, described in Section 3.1, unambiguously demonstrate the extreme efficiency of this multi-technique approach. Starting with EXAFS data, whose analysis is the most straightforward, one can highlight the main trends related to the Pd framework. First, is the evolution of interatomic distances, which were decreasing upon heating up to 250 °C and then started to increase upon further heating. The former fact will be discussed later (see Section 4.3), while the explanation of the latter is already possible with the help of the results of XANES analysis, which indicate that the increase of Pd-Pd distances is associated with the formation of palladium carbides based on the characteristic shape of the first XANES maximum. In such a process, carbon atoms occupy octahedral interstitial sites of palladium lattice, causing the lattice expansion [19,26,27,37–39]. This also explains the behavior of the Debye-Waller parameter. Indeed, its linear increase in the temperature range of 50–250 °C, which is above the Debye temperature for palladium [40], is in agreement with the correlated Debye model for monoatomic *fcc* system [41] (ignoring the fact of the additional structural disorder due to the nanometric dimensions). However, since the EXAFS Debye-Waller parameter accounts for both thermal and structural disorder effects, its non-linear increase above 250 °C should be associated with the latter, which can be explained by the incorporation of carbon impurities in the palladium lattice. Finally, it should be noted, that the spectra acquired in CO at room temperature are already different from the one collected for the initial metallic state of $Pd/Al_2O_3$ in He (Fig. S5a, blue lines) and already demonstrate carbide-like features, which can be explained by the sensitivity of XANES data to the surface-adsorbed CO molecules or carbon deposits (vide infra). The indirect evidence, that the observed shape is affected not only by the adsorbed CO but by mainly by the carbon deposits is that the broadening of the first maximum towards higher energies, typical for Pd-C bond [17–22], is observed gradually at 50 °C upon exposure to CO (Fig. S11), while the adsorption of CO molecules is expected to occur immediately. To further evidence the effect of interatomic distances, CO adsorption, surface carbon deposition and carbide formation on XANES spectra, theoretical XANES spectra were calculated (Fig. S8) for a set of geometries shown in Fig. S2. This allows giving a final interpretation of the MCR components shown in Fig. 1c as: Pd particle covered by CO and carbon deposits (blue), a similar Pd particle but with decreased interatomic distances (black) and Pd particle with increased interatomic distances and carbide formed in its bulk (red).

In DRIFTS data, the red shift of CO vibrations, and especially the bridge one, indicates that the reduction of surface Pd sites with to $Pd^{\sigma-}$, which is also reflected in XANES by a slight shift of the absorption edge. Finally, formation of palladium carbide, evidenced by XANES and EXAFS, together with the decrease of the bridge CO peak in DRIFTS, indicate that the disproportionation reaction $2CO \rightarrow CO_2 + C$ should take place [42,43], which is confirmed by the $CO_2$ signal in DRIFTS spectra around 2300 $cm^{-1}$ (Fig. S10). The difference in the temperature evolution of DRIFTS (Fig. 1h) and XAS (Fig. 1b,e) data can be explained by the fact, that the disproportionation reaction starts already at low temperatures according to the growth of the last (red) component and $CO_2$ signal in DRIFTS, while the active formation of the bulk palladium carbide according to XANES and EXAFS data starts only at ca. 250 °C, when the $CO_2$ signal (Fig. S10b) already reached saturated to its maximal value. A similar result was reported for $Pd/ZrO_2$ catalyst based on thermogravimetric and mass-spectrometry data compared to the *ex situ* XRD data [43]. The disproportionation reaction also explains the origin of carbon deposits, which were hypothetically observed in XANES spectra.

### 4.2. Evolution of $CH_4$ on palladium nanoparticles

Unlike CO, $CH_4$ shows no interaction with palladium at low temperatures, which is evident by its the XANES spectrum which does not show the carbide-like features at 50 °C (Fig. S5a). This is explained by the fact that activation of methane on palladium surface normally requires higher temperatures. However, small changes in the edge position may indicate a reductive effect of $CH_4$. The main effect observed upon heating is the decrease of Pd-Pd interatomic distances as also observed upon heating in CO. The three effects observed upon prolonged action of $CH_4$ at 350 °C, namely the increase of Pd-Pd interatomic distances, increase of the Debye-Waller and Pd-C features in XANES, unambiguously demonstrate that also in the case of $CH_4$ formation of palladium carbide takes place. Comparison of Pd nanoparticles' final states after CO and $CH_4$ (Fig. S8b) gases allows one to assert the same carbide structure in both cases. The final interpretation of the MCR components shown in Fig. 2c is the following: pure Pd particle (blue), a similar Pd particle but with decreased interatomic distances (black) and Pd particle with increased interatomic distances and carbide formed in its bulk (red). The above conclusions are also confirmed by PCA analysis of different combinations of the datasets (Fig. S7). In particular, the addition of the series in He (part d) and $CH_4$ (part f) to the series in CO leads to the same type of Scree plots since the number and type of expected structures in both cases is the same: pure particle, pure particle decreased interatomic distances, pure particle covered by CO/carbon deposits, a similar one with decreased distances, and palladium carbide.

### 4.3. Temperature-induced contraction of interatomic distances

The contraction of Pd-Pd distances observed upon heating in CO and $CH_4$ flow, also takes place during the heating in inert atmosphere for both carbon- and alumina-supported catalysts. This indicates that this contraction is a temperature effect, which occurred independently from the surface chemistry and the type of support (for carbon-supported sample, formation of palladium carbide was observed above 200 °C resulting to the lattice expansion which interfered with the initially started temperature induce lattice contraction). To understand this phenomenon, one should also consider that the contraction of metal–metal distances that is normally expected for nanosized particles [44] is not observed for palladium samples. The 3 nm particles, investigated in this work, in their metallic state after activation have exactly the same Pd-Pd distance of 2.74 Å as in the bulk palladium foil. The same was obtained for the smaller particles on P4VP support for which similar lattice contraction was also observed upon heating in CO and $CH_4$ gasses (Figs. S13–S14) but in the latter case to significantly lower values close to 2.70 Å, which is consistent with the smaller particle size. In several works, such unexpectedly high Pd-Pd distance in the nanosized samples was explained by the incorporation of impurities (H, C, N, O) into the palladium lattice as a result of the synthetic procedure [45,46]. Analyzing extensive number of literature reports, Santos *et al.* noted, that this effect is weaker for the supported samples, probably due to a spillover effect of the impurities from the particles to the support [45]. Following this idea, one can hypothesize that this effect can be further enhanced by the temperature. Our experiment also showed that cooling the sample back to 50 °C leads to a slight re-gain of the interatomic distances, which, however, remain smaller (2.73 Å) than the initial values. Another important fact is the reduction of palladium, which was confirmed by the shift of adsorbed CO vibration in DRIFTS data reported in Section 3.1, and by the edge shift in XANES towards lower energies for the sample heated in He (Section 3.3), which can possibly be related to metal-support charge transfer and also correlate with the hypothesis of spillover. Since the initial state of Pd was already considered as metallic $Pd^0$, the state formed upon heating should be assigned to $Pd^{\sigma-}$ one.

### 4.4. On the stability of surface and bulk palladium carbides

In a number of previous studies, we showed that hydrogen treatment can remove some of the surface adsorbates from palladium nanoparticles formed by interaction with hydrocarbons but does not affect bulk Pd carbides [18,21,37]. Since the removal of the carbide phase is of high potential importance in view of catalyst reactivation, we have tested the reversibility of palladium carbide formation in CO and $CH_4$ atmospheres by treating the samples in oxygen at different temperatures and subsequent treatment in hydrogen to reach again the metallic state of palladium. For the carbide-like phase formed at 50 °C in CO, subsequent purging with $O_2$ (to remove carbon deposits), He (to purge remaining oxygen) and $H_2$ to remove surface oxide at the same temperature leads to complete removal of carbide features in XANES spectrum. For the carbide phase formed in CO at 350 °C, the above treatment also leads to an almost complete removal of carbide features in XANES, however, only after repeating the oxygen treatment at 200 °C with subsequent reduction in $H_2$, the spectrum became fully identical to the initial metallic state.

## 5. Conclusion

This work provides a successful *in situ* characterization of supported palladium nanoparticles under various external conditions by a combination of EXAFS, XANES and DRIFTS spectroscopies, which can be further extended to numerous catalytic reactions over palladium involving CO. The following structural results were obtained:

- CO molecules are adsorbed on the surface of palladium and a disproportionation reaction with the formation of CO2 occurs already at low temperatures, with the saturation of the CO2 signal at ca. 230 °C.
- Formation of bulk palladium carbide in the above process starts only at temperatures above 250 °C.
- Decomposition of CH4 starts only at 350 °C and leads to the formation of palladium carbide phase similar to that observed in CO.
- Unusual contraction of Pd–Pd distances was observed upon heating irrespective of the gas atmosphere and the type of support, accompanied by the reduction of Pd to $Pd^{\sigma-}$ state.
- Both bulk carbide and surface carbon deposits can be removed by subsequent thermal treatment of palladium particles in O2 and H2 with the formation of metallic Pd.

The knowledge of how atomic and electronic structure of palladium is affected by CO and $CH_4$ as function of time and temperature may give valuable insights on the behavior of numerous catalytic reactions which either focus on the direct conversion of CO and $CH_4$ or may have them as potential reaction intermediates.

## CRediT authorship contribution statement

**Oleg A. Usoltsev:** Software, Writing – original draft. **Alina A. Skorynina:** Visualization. **Bogdan O. Protsenko:** Software, Validation. **Vlad Martin-Diaconescu:** Investigation. **Riccardo Pellegrini:** Investigation. **Alexander V. Soldatov:** Funding acquisition. **Jeroen van Bokhoven:** Data curation, Writing – review & editing. **Aram L. Bugaev:** Conceptualization, Methodology.

## Declaration of Competing Interest

The authors declare the following financial interests/personal relationships which may be considered as potential competing interests: Aram L. Bugaev, Alina A. Skorynina, Alexander V. Soldatov reports financial support was provided by Russian Foundation for Basic Research.

## Data availability

Data will be made available on request.

## Acknowledgements

O.A.U., A.A.S., A.V.S. and A.L.B. acknowledge the Ministry of Science and Higher Education of the Russian Federation for financial support (Agreement № 075-15-2021-1389 from 13.10.2021). We acknowledge ALBA synchrotron and the stuff of CLAESS beamline for providing the beamtime and the support during the experiment. Theoretical calculation of XANES spectra was performed using the Blokhin HPC of the Center for collective use "Nanoscale Structure of Matter" of the Southern Federal University.

## Appendix A. Supplementary material

Supplementary data to this article can be found online at https://doi.org/10.1016/j.apsusc.2022.156171.

## References

[1] Y. He, C. Luan, Y. Fang, X. Feng, X. Peng, G. Yang, N. Tsubaki, Low-temperature direct conversion of methane to methanol over carbon materials supported Pd-Au nanoparticles, Catal. Today 339 (2020) 48–53.
[2] J. Chen, S. Wang, L. Peres, V. Collière, K. Philippot, P. Lecante, Y. Chen, N. Yan, Oxidation of methane to methanol over Pd@Pt nanoparticles under mild conditions in water, Catal. Sci. Technol. 11 (2021) 3493–3500.
[3] X. Li, X. Wang, K. Roy, J.A. van Bokhoven, L. Artiglia, Role of water on the structure of palladium for complete oxidation of methane, ACS Catal. 10 (2020) 5783–5792.
[4] P. Velin, F. Hemmingsson, A. Schaefer, M. Skoglundh, K.A. Lomachenko, A. Raj, D. Thompsett, G. Smedler, P.A. Carlsson, Hampered PdO redox dynamics by water suppresses lean methane oxidation over realistic palladium catalysts, ChemCatChem 13 (2021) 3765–3771.
[5] N.M. Martin, J. Nilsson, M. Skoglundh, E.C. Adams, X. Wang, P. Velin, G. Smedler, A. Raj, D. Thompsett, H.H. Brongersma, T. Grehl, G. Agostini, O. Mathon, S. Carlson, K. Norén, F.J. Martinez-Casado, Z. Matej, O. Balmes, P.-A. Carlsson, Characterization of surface structure and oxidation/reduction behavior of Pd–Pt/$Al_2O_3$ model catalysts, J. Phys. Chem. C 120 (2016) 28009–28020.
[6] L. Li, S. Xue, M. Wei, H. Yao, Y. Dai, Z. Fei, Ultrafine Pd species anchored on porous $CeO_2$ nanobundles as a highly efficient catalyst for methane oxidation, Appl. Surf. Sci. 599 (2022).
[7] P. Velin, M. Ek, M. Skoglundh, A. Schaefer, A. Raj, D. Thompsett, G. Smedler, P.-A. Carlsson, Water inhibition in methane oxidation over alumina supported palladium catalysts, J. Phys. Chem. C 123 (2019) 25724–25737.
[8] H. Cui, Z. Liu, P. Jia, Pd-doped $C_3N$ monolayer: a promising low-temperature and high-activity single-atom catalyst for CO oxidation, Appl. Surf. Sci. 537 (2021).
[9] S. Tang, L. Xu, B. Peng, F. Xiong, T. Chen, X. Luo, X. Huang, H. Li, J. Zeng, Z. Ma, L.-L. Wang, Ga-doped Pd/$CeO_2$ model catalysts for CO oxidation reactivity: a density functional theory study, Appl. Surf. Sci. 575 (2022).
[10] G.L. Chiarello, Y. Lu, M. Agote-Arán, R. Pellegrini, D. Ferri, Changes of Pd oxidation state in Pd/$Al_2O_3$ catalysts using modulated excitation DRIFTS, Catalysts 11 (2021) 116.
[11] V. Muravev, J.F.M. Simons, A. Parastaev, M.A. Verheijen, J.J.C. Struijs, N. Kosinov, E.J.M. Hensen, Operando spectroscopy unveils the catalytic role of different palladium oxidation states in CO oxidation on Pd/$CeO_2$ catalysts, Angew. Chem. Int. Ed. 61 (2022) e202200434.
[12] C. Ahoba-Sam, E. Borfecchia, A. Lazzarini, A. Bugaev, A.A. Isah, M. Taoufik, S. Bordiga, U. Olsbye, On the conversion of $CO_2$ to value added products over composite PdZn and H-ZSM-5 catalysts: excess Zn over Pd, a compromise or a penalty? Catal. Sci. Technol. 10 (2020) 4373–4385.
[13] A. Ramirez, P. Ticali, D. Salusso, T. Cordero-Lanzac, S. Ould-Chikh, C. Ahoba-Sam, A.L. Bugaev, E. Borfecchia, S. Morandi, M. Signorile, S. Bordiga, J. Gascon, U. Olsbye, Multifunctional catalyst combination for the direct conversion of $CO_2$ to propane, JACS Au 1 (2021) 1719–1732.
[14] C. Vogt, F. Meirer, M. Monai, E. Groeneveld, D. Ferri, R.A. van Santen, M. Nachtegaal, R.R. Unocic, A.I. Frenkel, B.M. Weckhuysen, Dynamic restructuring of supported metal nanoparticles and its implications for structure insensitive catalysis, Nat. Commun. 12 (2021) 7096.
[15] V. Muravev, G. Spezzati, Y.-Q. Su, A. Parastaev, F.-K. Chiang, A. Longo, C. Escudero, N. Kosinov, E.J.M. Hensen, Interface dynamics of Pd–$CeO_2$ single-atom catalysts during CO oxidation, Nat. Catal. 4 (2021) 469–478.
[16] F.A. Lewis, The palladium/hydrogen system, 1967.
[17] A.L. Bugaev, A.A. Guda, K.A. Lomachenko, V.V. Shapovalov, A. Lazzarini, J. G. Vitillo, L.A. Bugaev, E. Groppo, R. Pellegrini, A.V. Soldatov, J.A. van Bokhoven, C. Lamberti, Core–shell structure of palladium hydride nanoparticles revealed by combined X-ray absorption spectroscopy and X-ray diffraction, J. Phys. Chem. C 121 (2017) 18202–18213.

[18] A.L. Bugaev, O.A. Usoltsev, A.A. Guda, K.A. Lomachenko, I.A. Pankin, Y. V. Rusalev, H. Emerich, E. Groppo, R. Pellegrini, A.V. Soldatov, J.A. van Bokhoven, C. Lamberti, Palladium carbide and hydride formation in the bulk and at the surface of palladium nanoparticles, J. Phys. Chem. C 122 (2018) 12029–12037.
[19] A.L. Bugaev, O.A. Usoltsev, A.A. Guda, K.A. Lomachenko, M. Brunelli, E. Groppo, R. Pellegrini, A.V. Soldatov, J. van Bokhoven, Hydrogenation of ethylene over palladium: evolution of the catalyst structure by operando synchrotron-based techniques, Faraday Discuss. 229 (2021) 197–207.
[20] J. Vercammen, M. Bocus, S. Neale, A. Bugaev, S. Van Minnebruggen, J. Hajek, P. Tomkins, A. Soldatov, A. Krajnc, G. Mali, V. Van Speybroeck, D.E. De Vos, Shape-selective C-H activation of aromatics to biarylic compounds using molecular palladium in zeolites, Nat. Catal. 3 (2020) 1002–1009.
[21] A.L. Bugaev, A.A. Guda, A. Lazzarini, K.A. Lomachenko, E. Groppo, R. Pellegrini, A. Piovano, H. Emerich, A.V. Soldatov, L.A. Bugaev, V.P. Dmitriev, J.A. van Bokhoven, C. Lamberti, In situ formation of hydrides and carbides in palladium catalyst: when XANES is better than EXAFS and XRD, Catal. Today 283 (2017) 119–126.
[22] A.A. Guda, S.A. Guda, K.A. Lomachenko, M.A. Soldatov, I.A. Pankin, A.V. Soldatov, L. Braglia, A.L. Bugaev, A. Martini, M. Signorile, E. Groppo, A. Piovano, E. Borfecchia, C. Lamberti, Quantitative structural determination of active sites from in situ and operando XANES spectra: from standard ab initio simulations to chemometric and machine learning approaches, Catal. Today 336 (2019) 3–21.
[23] A.L. Bugaev, A.A. Guda, K.A. Lomachenko, V.V. Srabionyan, L.A. Bugaev, A. V. Soldatov, C. Lamberti, V.P. Dmitriev, J.A. van Bokhoven, Temperature- and pressure-dependent hydrogen concentration in supported $PdH_x$ nanoparticles by Pd K-edge X-ray absorption spectroscopy, J. Phys. Chem. C 118 (2014) 10416–10423.
[24] D. Narehood, S. Kishore, H. Goto, J. Adair, J. Nelson, H. Gutierrez, P. Eklund, X-ray diffraction and H-storage in ultra-small palladium particles, Int. J. Hydrogen Energ. 34 (2009) 952–960.
[25] A.L. Bugaev, M. Zabilskiy, A.A. Skorynina, O.A. Usoltsev, A.V. Soldatov, J.A. van Bokhoven, In situ formation of surface and bulk oxides in small palladium nanoparticles, Chem. Commun. 56 (2020) 13097–13100.
[26] O.A. Usoltsev, A.L. Bugaev, A.A. Guda, S.A. Guda, A.V. Soldatov, Absorption of hydrocarbons on palladium catalysts: from simple models towards machine learning analysis of X-ray absorption spectroscopy data, Top. Catal. 63 (2020) 58–65.
[27] O.A. Usoltsev, A.Y. Pnevskaya, E.G. Kamyshova, A.A. Tereshchenko, A. A. Skorynina, W. Zhang, T. Yao, A.L. Bugaev, A.V. Soldatov, Dehydrogenation of ethylene on supported palladium nanoparticles: a double view from metal and hydrocarbon sides, Nanomaterials 10 (2020) 1643.
[28] O.A. Usoltsev, A.L. Bugaev, A.A. Guda, S.A. Guda, A.V. Soldatov, How much structural information could be extracted from XANES spectra for palladium hydride and carbide nanoparticles, J. Phys. Chem. C 126 (2022) 4921–4928.
[29] L. Simonelli, C. Marini, W. Olszewski, M. Ávila Pérez, N. Ramanan, G. Guilera, V. Cuartero, K. Klementiev, CLÆSS: the hard X-ray absorption beamline of the ALBA CELLS synchrotron, Cogent. Phys. 3 (2016) 1231987.
[30] M. Newville, Larch: an analysis package for XAFS and related spectroscopies, J. Phys. Conf. Ser. 430 (2013) 012007.
[31] S.I. Zabinsky, J.J. Rehr, A. Ankudinov, R.C. Albers, M.J. Eller, Multiple-scattering calculations of X-ray-absorption spectra, Phys. Rev. B 52 (1995) 2995–3009.
[32] J.J. Rehr, R.C. Albers, Theoretical approaches to x-ray absorption fine structure, Rev. Mod. Phys. 72 (2000) 621–654.
[33] A. Martini, S.A. Guda, A.A. Guda, G. Smolentsev, A. Algasov, O. Usoltsev, M. A. Soldatov, A. Bugaev, Y. Rusalev, C. Lamberti, A.V. Soldatov, PyFitit: the software for quantitative analysis of XANES spectra using machine-learning algorithms, Comput. Phys. Commun. 250 (2020), 107064.
[34] S.A. Guda, A.A. Guda, M.A. Soldatov, K.A. Lomachenko, A.L. Bugaev, C. Lamberti, W. Gawelda, C. Bressler, G. Smolentsev, A.V. Soldatov, Y. Joly, Optimized finite difference method for the full-potential XANES simulations: application to molecular adsorption geometries in MOFs and metal–ligand intersystem crossing transients, J. Chem. Theor. Comput. 11 (2015) 4512–4521.
[35] A.A. Guda, S.A. Guda, M.A. Soldatov, K.A. Lomachenko, A.L. Bugaev, C. Lamberti, W. Gawelda, C. Bressler, G. Smolentsev, A.V. Soldatov, Y. Joly, Finite difference method accelerated with sparse solvers for structural analysis of the metal-organic complexes, J. Phys. Conf. Ser. 712 (2016), 012004.
[36] S.D. Ebbesen, B.L. Mojet, L. Lefferts, The influence of water and pH on adsorption and oxidation of CO on $Pd/Al_2O_3$ - an investigation by attenuated total reflection infrared spectroscopy, PCCP 11 (2009) 641–649.
[37] A.L. Bugaev, A.A. Guda, I.A. Pankin, E. Groppo, R. Pellegrini, A. Longo, A. V. Soldatov, C. Lamberti, The role of palladium carbides in the catalytic hydrogenation of ethylene over supported palladium nanoparticles, Catal. Today 336 (2019) 40–44.
[38] A.A. Skorynina, A.A. Tereshchenko, O.A. Usoltsev, A.L. Bugaev, K.A. Lomachenko, A.A. Guda, E. Groppo, R. Pellegrini, C. Lamberti, A.V. Soldatov, Time-dependent carbide phase formation in palladium nanoparticles, Radiat. Phys. Chem. 175 (2020), 108079.
[39] W. Stuyck, A.L. Bugaev, T. Nelis, R. de Oliveira-Silva, S. Smolders, O.A. Usoltsev, D. Arenas Esteban, S. Bals, D. Sakellariou, D. De Vos, Sustainable formation of tricarballylic acid from citric acid over highly stable $Pd/Nb_2O_5.nH_2O$ catalysts, J. Catal. 408 (2022) 88–97.
[40] J.S. Brown, Note on the Debye temperature of palladium, J. Phys. C Solid State Phys. 3 (1970) L175–L177.
[41] G. Beni, P.M. Platzman, Temperature and polarization dependence of extended X-ray absorption fine-structure spectra, Phys. Rev. B 14 (1976) 1514–1518.
[42] C.L.M. Joyal, J.B. Butt, Chemisorption and disproportionation of carbon monoxide on palladium/silica catalysts of differing percentage metal exposed, J. Chem. Soc. Faraday Trans. 1 (1987) 83.
[43] M. Maciejewski, A. Baiker, Incorporation and reactivity of carbon in palladium, Pure Appl. Chem. 67 (1995) 1879–1884.
[44] W.H. Qi, M.P. Wang, Size and shape dependent lattice parameters of metallic nanoparticles, J. Nanopart. Res. 7 (2005) 51–57.
[45] E.G. Ciapina, M.L. dos Santos, R.M.I.S. Santos, J. Palombarini, O.P. Almeida Júnior, J.C.C.d.C. Santana, D.A. Modesto, A.J.C. Lanfredi, S.F. Santos, On the lattice dilation of palladium nanoparticles and a new methodology for the quantification of interstitials, J. Alloys Compd. 881 (2021) 160628.
[46] T. Ohba, H. Kubo, Y. Ohshima, Y. Makita, N. Nakamura, H. Uehara, S. Takakusagi, K. Asakura, EXAFS studies of Pd nanoparticles: direct evidence for unusual Pd–Pd bond elongation, Chem. Lett. 44 (2015) 803–805.